The Reduction Potential of Cytochrome b_5 Is Modulated by Its Exposed Heme Edge[†]

Mario Rivera,*[,‡] Rajalakshmi Seetharaman,[‡] Deepak Girdhar,[‡] Marc Wirtz,[‡] Xuejun Zhang,[§] Xioqiang Wang,[§] and Steven White[||]

Department of Chemistry, Oklahoma State University, Stillwater, Oklahoma 74078-3071, Crystallography Program, Oklahoma Medical Research Foundation, 825 NE 13th Street, Oklahoma City, Oklahoma 73104, and Department of Biochemistry and Molecular Biology, Oklahoma State University, Stillwater, Oklahoma 74078-3071

Received September 26, 1997; Revised Manuscript Received November 13, 1997

ABSTRACT: When the reduction potential of cytochrome b_5 is measured with the aid of several different surface-modified electrodes that function on the basis of electrostatic interactions with the protein, the resultant values have been consistently more positive (40−100 mV) than the reduction potentials measured with potentiometric methods. In this paper, we report that the heme edge containing the exposed heme propionate, a heme methyl, and a heme vinyl, and which constitutes part of the surface of cytochrome b_5, modulates its reduction potential. The positive shifts observed in the voltammetric measurements appear to originate from the formation of a complex between cytochrome b_5 and the modified electrode surface which (a) neutralizes the charge on the heme propionate located on the exposed heme edge and (b) lowers the dielectric of the exposed heme microenvironment by excluding water from the complex interface, factors which result in the destabilization of the positive charge on the ferric heme with respect to the neutral ferrous heme. The observed positive shift, which is induced by complexation at the electrode surface, may indicate that similar shifts in the reduction potential of cytochrome b_5 occur when it forms a complex with physiological partners, prior to electron transfer. The effect of the value of the dielectric constant on the reduction potential of cytochrome b_5 was corroborated by preparing the V45L/V61L double mutant whose reduction potential was measured to be 50 mV more negative than the value measured for the wild type protein. The negative shift in the reduction potential of the mutant protein was explained by the increased accessibility of water to the heme binding site, as observed in its X-ray crystal structure.

The first reports on the use of modified electrodes aimed at obtaining reversible electrochemistry of cytochrome *c* (cyt *c*) were related to the use of 4,4′-bipyridine as a modifier (*1*, *2*) and the use of bis(4-pyridyl)disulfide (*3*, *4*). These early reports sparked an intense effort aimed at understanding several important aspects of the direct cyclic voltammetry of redox proteins at functionalized electrodes, including the role played by the electrode modifiers in promoting the reversible voltammetry of redox proteins, potential molecular recognition between the electrode and protein surfaces, and reversibility of the electrode−protein association, to name a few. These research efforts have been recently reviewed by Armstrong (*5*), Bond (*6*), and Hawkridge and Taniguchi (*7*). Subsequent studies aimed at observing the reversible electrochemistry of small redox proteins other than cyt *c* were largely based on the fact that most electron-transfer proteins recognize one another electrostatically.

In contrast to the extensively studied cyt *c*, a large number of small electron-transfer proteins have negative electrostatic fields near their active sites. The direct electrochemistry of these proteins has been promoted by a variety of experimental schemes, for example, the HS−R−X motif, in which the thiol group is used to form self-assembled monolayers on an electrode surface, where X represents a basic group such as a protonated amine that provides a means for electrostatic recognition between the negatively charged protein and the modified electrode, and where R represents an aliphatic or aromatic spacer. Examples of these types of surface-modified electrodes include those modified with 2-aminoethane (*8*, *9*) and those modified with peptides such as $(Lys\text{-}Cys)_2$ (*10*) which were used to promote the reversible electrochemistry of plastocyanin and cyt b_5 at gold electrodes. The use of negatively charged edge pyrolytic graphite electrodes to promote the electrochemistry of negatively charged proteins has also been reported (*11*−*13*). Electrochemical communication between the negatively charged protein and the pyrolytic carbon surfaces was promoted by addition of divalent or trivalent cations, such as Ca^{2+}, Mg^{2+}, or $Cr[(NH_3)_6]^{3+}$. More recently, Rivera et al. (*14*) reported a variation of this approach which consists of modifying a polycrystalline gold disk electrode with a self-assembled monolayer of β-mercaptopropionate. Electrochemical communication between the negatively charged electrode and the negatively charged cytochrome b_5 (cyt b_5) was achieved by

[†] The financial support of Grants NIH GM 50503 and AHA 9507904S is gratefully acknowledged. Funds for the 400 MHZ spectrometer of the Oklahoma Statewide Shared NMR Facility were provided by the National Science Foundation (Grant BIR-9512269), the Oklahoma State Regents for Higher Education, the W. W. Keck Foundation, and Conoco, Inc. The authors are also indebted to Cambridge Isotope Laboratories for a CIL Research Grant.

* To whom correspondence should be addressed.

[‡] Department of Chemistry, Oklahoma State University.

[§] Oklahoma Medical Research Foundation.

[||] Department of Biochemistry and Molecular Biology, Oklahoma State University.

S0006-2960(97)02390-8 CCC: $15.00
Published on Web 01/22/1998

addition of polylysine, or multivalent cations (Ca^{2+}, Mg^{2+}, or $[Cr(NH_3)_6]^{3+}$) to the solution contained in the electrochemical cell. Glenn and Bowden (*15*) have reported the diffusionless electrochemistry of cyt b_5 adsorbed on a multilayer film electrode consisting of 8-mercaptooctanoate and polylysine.

A feature common to all voltammetric experiments involving cyt b_5 and the electrodes described above is that the reduction potential measured with direct electrochemistry is significantly more positive than the reduction potential measured with equilibrium techniques. For example, Bagby et al. (*10*) reported that the reduction potential of beef microsomal cyt b_5 observed at gold electrodes modified with the peptides Cys-Lys-Cys, Arg-Cys, and His-Cys is 40 mV more positive than the value measured by spectroelectrochemistry. Rivera et al. (*14*) reported that, when the electrochemistry of cyt b_5 is promoted by polylysine at a β-mercaptopropionate-modified electrode, the reduction potentials of beef liver microsomal cyt b_5 and recombinant rat outer mitochondrial membrane (OM) cyt b_5 are substantially more positive than their corresponding values measured by potentiometry. Furthermore, these authors also reported that the reduction potentials become increasingly more positive as the concentration of polylysine in the electrochemical cell is increased. Glenn and Bowden (*15*) also reported that, when the diffusionless electrochemistry of recombinant beef microsomal cyt b_5 is promoted at a multilayer film electrode consisting of 8-mercaptooctanoate and polylysine, the observed reduction potential is approximately 50 mV more positive than the value measured with spectroelectrochemistry. By comparison, when similar electrodes are used to measure the reduction potential of other negatively charged proteins, such as ferredoxin and plastocyanin, the values measured by voltammetry and spectroelectrochemistry are in good agreement (*2*, *11*−*13*).

It is therefore apparent that there is something unique about the interaction between cyt b_5 and modified electrodes that results in reduction potentials that are significantly more positive than the reduction potential values measured with potentiometric techniques. The electrostatic recognition between modified electrode and protein, which precedes heterogeneous electron transfer in voltammetric experiments, has been compared to the electrostatic interactions that occur between physiological partner proteins just before electrons are transferred from one protein to another in homogeneous solution (*2*, *16*). For this reason, the significant anodic shift observed in the reduction potential of cyt b_5 when it is measured at surface-modified electrodes that rely upon electrostatic interactions may be indicative of important structure−function relationships in this heme protein. Furthermore, because of the increasing popularity of voltammetric methods in measuring the reduction potential of the wild type and site-directed mutants, a sound understanding of the factors responsible for the unusual behavior of cyt b_5 at modified surfaces is necessary.

EXPERIMENTAL PROCEDURES

Recombinant rat liver outer mitochondrial membrane (OM) cyt b_5 was expressed in *Escherichia coli* and purified as described previously (*17*). Polylysine with a MW of 3970, and 9000, determined using viscosity measurements, was purchased from Sigma and was used without further purification. All other reagents were purchased from Aldrich or Sigma and were used as received.

Cyclic Voltammetry. Cyclic voltammetry was carried out with a BAS-CV50W potentiostat (Bioanalytical Systems). A miniature 1 mm diameter gold disk working electrode, a platinum wire counter electrode, and an Ag/AgCl reference electrode equipped with a fiber junction were purchased from Cypress Systems. All electrodes were placed in a single-compartment glass cell of approximately 700 μL. Before each experiment, the working electrode was successively polished using 15, 6, and 1 μm diamond polishing slurries on nylon followed by polishing with 0.05 μm alumina polishing slurry on cotton wool, then thoroughly washed with deionized water, and sonicated for 3 min in deionized water. Surface modification of the electrode was achieved by dipping the polished gold working electrode into a 100 mM solution of β-mercaptopropionate for 20 min, followed by rinsing with deionized water. The modified electrode was then immediately immersed in a deaerated protein solution, and a stream of nitrogen was blown gently across the surface of the protein solution in order to keep the solution anaerobic. Protein concentrations were typically 100 μM, and their concentrations were measured by UV−vis spectrophotometry using the Soret band corresponding to their oxidized state. The extinction coefficient (ϵ_{412}) used for OM cyt b_5 and its dimethyl ester derivative is 130 mM^{-1} cm^{-1} (*18*). The concentration of polylysine was obtained from the weight of substance weighed using the average molecular weight provided by Sigma. Titrations monitored by cyclic voltammetry were performed immediately after the electrode surface was modified. Between data points, the working electrode was rinsed with deionized water and then immersed in a 100 mM solution of β-mercaptopropionate for 5 min in order to avoid deterioration of the modified surface throughout the experiment. Although reduction potentials were obtained with respect to a silver/silver chloride electrode, all values reported in this paper are with respect to the standard hydrogen electrode.

Preparation of didodecyldimethylammonium bromide (DDAB) films on mini glassy carbon electrodes, 1 mm diameter (Cypress Systems), was carried out according to the protocol described by Tominaga et al. (*19*). The glassy carbon electrodes were polished, rinsed, and sonicated as described above. The electrode was subsequently dried at room temperature and then immersed for 10 s in a 0.05 M solution of DDAB in chloroform, kept at 4 °C. The electrode was subsequently dried at room temperature for 30 min and then immersed in the electrochemical cell containing 250 μL of protein thermostated at 22 °C. Protein was incorporated into the DDAB film on the electrode surface by repeated potential cycling until the magnitude of the current remained constant.

Spectroelectrochemistry. Transmission mode spectroelectrochemical titrations were carried out in cell bodies constructed of polyacrylate that had an optically transparent gold minigrid (200 wires/in., 70% transmittance, Buckbee Mears Co., St. Paul, MN), quartz windows, a gold minigrid counter electrode, and a compartment for the Ag/AgCl reference electrode. The details of the spectroelectrochemical cell and titrations have been reported elsewhere (*20*). For OM cyt b_5, the spectra of fully reduced and fully oxidized protein

were obtained at −550 and −70 mV (vs Ag/AgCl), respectively. Spectra were recorded at 20 mV intervals between these two potentials. The solutions prepared for spectroelectrochemistry contained 0.30 mM $[Ru(NH_3)_6]Cl_3$, 1.41 mM methyl viologen, and 0.052 mM protein in MOPS buffer at pH 7.0.

NMR Spectroscopy. ^{13}C-labeled δ-aminolevulinic acid (ALA) was used to prepare the ^{13}C-labeled hemes incorporated into OM cyt b_5. Details of the synthesis of [1-^{13}C]-ALA have been reported elsewhere (*21*, *22*). OM cyt b_5 labeled with ^{13}C at the heme active site was obtained and purified to homogeneity utilizing the method described by Rivera and Walker (*23*). Titrations of OM cyt b_5 with polylysine were carried out with a Varian Unitiy Inova 400 spectrometer operating at a ^{13}C frequency of 100.6 MHz. Typically, OM cyt b_5 solutions (2 mM) were prepared in 5 mM perdeuterated phosphate buffer at pH 7.0 (not corrected for the isotope effect). OM cyt b_5 used in the titration experiments was exhaustively dialyzed against water, exchanged with D_2O, and subsequently freeze-dried. Titration experiments monitored with resonances attributed to heme propionate carbonyl carbons were acquired at 30 °C with a spectral width of 9.5 kHz, 21K data points, a 1.1 s acquisition time, and a 200 ms relaxation delay. Typically, 2000−3000 scans were acquired for each point in the titration curve.

Site-Directed Mutagenesis. The transformer site-directed mutagenesis kit (Clonetech) and the recombinant plasmid MRL1 (*17*) were used to construct all mutants. The sequences corresponding to the mutagenic primers designed to introduce mutations V61L and V45L and that corresponding to the selection primer (*Afl*III to *Bgl*II) are 5′-CCGAATCTTTCGAAGATCTGGGCCACTCTCCGGATGCGCG-3′, 5′-CCCGGGCGGCGAAGAACTGCTGCTGGAACAGGCGGGC-3′, and 5′-GGGGATAACGCAGGAAAGAAGATCTGAGCAAAAGGCC-3′, respectively. The underlined codons represent mismatches introduced to generate the mutations. Mutations V61L and V45L remove the *Xmn*I and *Msc*I restriction sites, respectively. The V61L mutant was constructed with the corresponding mutagenic and selection primer, and the double mutant was constructed with the two mutagenic and selection primers used simultaneously. The mutated gene was then separated from the pBS+ plasmid by digesting with *Bam*HI and *Nde*I and then purified with the aid of agarose gel electrophoresis. The 300-base pair gene was subsequently cloned into the expression vector pET 11a, as described previously (*17*). The mutants were screened both by determining the absence of the corresponding restriction site and by automated sequencing using an Applied Biosystems 373 DNA sequencer. The recombinant pET construct was transformed into *E. coli* BL21(DE3) cells, and the proteins were expressed and purified as described previously (*17*).

Crystal Growth and X-ray Crystallography Data Collection. X-ray quality crystals of the V45L/V61L mutant of OM cyt b_5 were grown using the vapor diffusion method utilizing conditions similar to those used to grow crystals of the wild type protein (*24*). In brief, protein was dissolved in 20 mM TRIS and 0.1% sodium azide (pH 7.8) to produce a solution containing 20 mg of protein/mL. This solution was mixed with well solution [30% polyethylene glycol (MW = 8000), 0.20 M magnesium acetate, and 0.10 PIPES buffer (pH 6.8)]. The crystals grew to dimensions of 1 mm × 0.3 mm × 0.3 mm in approximately 1 month. The crystal belongs to space group $P2_12_12_1$ and diffracts to 2.0 Å resolution.

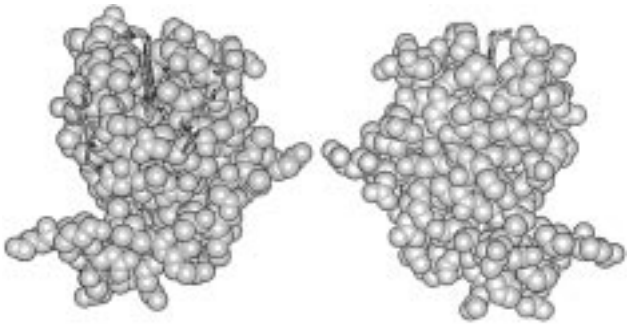

FIGURE 1: (Left) View of the exposed heme edge in cyt b_5. The heme, the acidic residues, and the axial ligands are shown in stick rendering. The area delineated by the exposed heme propionate, Glu48, Glu44, Asp60, and Glu56 (clockwise) is known to participate in electrostatic complexes formed by cyt b_5 and cyt *c*. (Right) View of the buried heme edge in cyt b_5. This view was obtained by rotating the view presented on the left by 180° about the vertical axis of the page.

Preparation of the Dimethyl Ester of Cytochrome b_5. The dimethyl ester of cyt b_5 was prepared utilizing previously reported methodology (*25*, *26*).

RESULTS AND DISCUSSION

Spectroelectrochemistry. The three-dimensional structure of beef liver microsomal cyt b_5 (*27*) and OM cyt b_5 (*24*) shows that one edge of the heme is almost entirely exposed to the aqueous environment (Figure 1), while the opposite edge is entirely buried in the hydrophobic heme binding pocket. On the basis of molecular modeling (*28*, *29*) and site-directed mutagenesis studies (*30*), amino acids Glu44, Glu48, Glu56, and Asp60 were identified to be the acidic residues on the surface of cyt b_5 that participate in the electrostatic binding between cyt b_5 and cyt *c*. More recently, ^{13}C NMR spectroscopic studies provided experimental evidence that the heme propionate located on the exposed heme edge of cyt b_5 also participates in the electrostatic binding to cyt *c* (*24*). Consequently, it is well-known that cyt b_5 binds with redox partners utilizing the surface area delimited by acidic residues 44, 48, 56, and 60 and the heme propionate located on the exposed heme edge (Figure 1).

Rivera et al. (*14*) reported that, when the cyclic voltammogram of cyt b_5 is obtained at a β-mercaptopropionate-modified gold electrode in the presence of polylysine as a promoter, the reduction potential of the cyt shifts in the positive direction as the concentration of polylysine is increased. This unusual behavior was attributed to the formation of a complex between polylysine and cyt b_5 at the electrode surface. To investigate the nature of this shift in more detail, the reduction potential of cyt b_5 was measured by spectroelectrochemistry in the presence and in the absence of polylysine. The results of these experiments are summarized in Table 1. When the reduction potential of cyt b_5 is measured in the presence of polylysine (polylysine/cyt b_5 mole ratio = 2.0), its reduction potential is 30 mV (polylysine MW = 3970) and 62 mV (polylysine MW = 9000) more positive than the value measured in the absence of polylysine, respectively (Table 1). By comparison, when similar experiments were performed with the dimethyl ester of cyt b_5,

Table 1: Reduction Potentials Obtained by Spectroelectrochemistry[a]

protein	polylysine (MW = 3970)	polylysine (MW = 9000)	$E°$ (mV)
cyt b_5 (47 μM)	−	−	−102
cyt b_5 (52 μM)	103 μM	−	−70
cyt b_5 (52 μM)	−	104 μM	−40
DiMe b_5 (52 μM)	−	−	−36
DiMe b_5 (52 μM)	104 μM	−	−33
DiMe b_5 (52 μM)	−	104 μM	−32

[a] cyt b_5 = OM cyt b_5. DiMe b_5 = OM cyt b_5 dimethyl ester.

DiMe cyt b_5, the reduction potentials measured are independent of the presence of polylysine in the spectroelectrochemical cell (Table 1).

The 66 mV difference between the reduction potentials of OM cyt b_5 and its DiMe ester can be explained by the stabilization of the positive charge of the ferric heme in OM cyt b_5 by the heme propionates. This stabilization is no longer possible in the DiMe derivative, and consequently, its reduction potential becomes more positive (*26*, *31*).

An important feature of the spectroelectrochemical experiment is that electrons are transferred from the electrode to the protein via redox mediators, and consequently, the protein is not in intimate contact with the electrode during the oxidation or reduction process. Therefore, the positive shift in the reduction potential of OM cyt b_5 in the presence of polylysine (Table 1) must arise from the formation of a complex between the protein and polylysine. By comparison, the reduction potential of the DiMe derivative is not affected by the presence of polylysine in solution, thus indicating that the shift in reduction potential observed for cyt b_5 in the presence of polylysine must result from the electrostatic neutralization of the heme propionate located on the exposed heme edge. The values of the reduction potential of DiMe cyt b_5, which are independent of the concentration of polylysine (Table 1), also indicate that neutralization of the acidic residues on the surface of the protein upon complexation with polylysine does not have a large effect on its reduction potential. The latter is in agreement with reports indicating that elimination of the negative charge of residues 44, 48, 56, and 60 does not have an effect on the reduction potential of the mutants (*32*). Evidence for the formation of a complex between DiMe cyt b_5 and polylysine is provided by the fact that polylysine promotes the voltammetry of DiMe cyt b_5 (see the next section), but since the heme propionate on the exposed heme edge of the ester derivative cannot participate in electrostatic binding, its reduction potential, measured by spectroelectrochemistry, is not affected (Table 1).

Additional evidence for the participation of the heme propionate located on the exposed heme edge of cyt b_5 in binding to polylysine comes from ^{13}C NMR experiments. To this end, the heme propionate carbonyl carbons in cyt b_5 were labeled with ^{13}C utilizing a previously described method (*23*, *24*). The ^{13}C NMR spectrum of OM cyt b_5 whose heme has been enriched at the carbonyl carbons is shown in Figure 2. The four carbonyl resonances result from the heme isomerism observed in cytochromes b_5. In OM cyt b_5, isomers A and B coexist in solution with an isomer ratio (A/B) of 1/1 (*17*). The assignment of the ^{13}C resonances corresponding to the two heme orientation isomers in ferricytochrome b_5 has been described previously (*24*). In

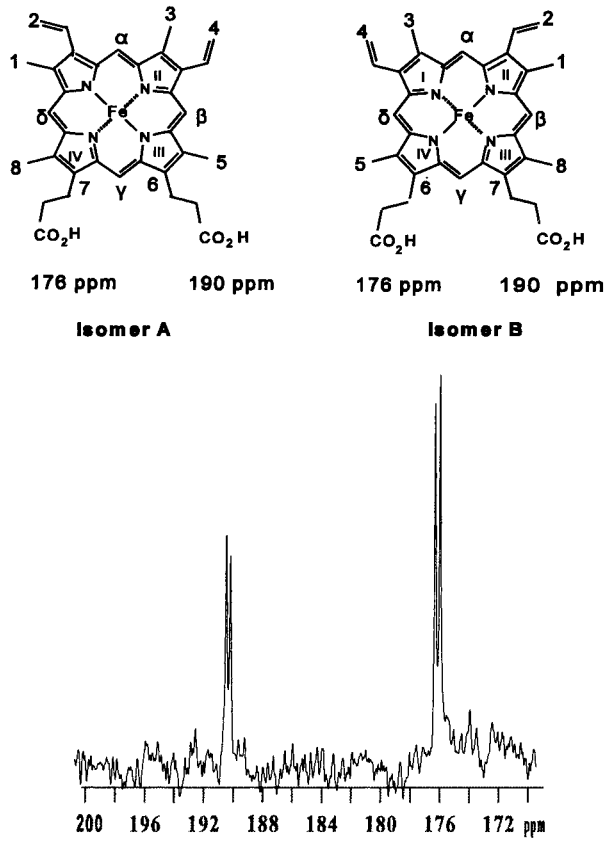

FIGURE 2: When the heme in cyt b_5 is labeled with [1-^{13}C]ALA, isotopic incorporation occurs exclusively at the heme propionate carbonyl carbons. The ^{13}C NMR spectrum of the labeled protein displays four peaks due to the two heme isomers present in solution which differ by a 180° rotation about the α,γ-meso axis. The carbonyl resonances arising from the exposed heme propionate, A6 CO and B7 CO, are located near 190 ppm, and those arising from the buried heme edge, A7 CO and B6 CO, are located near 176 ppm. The chemical shift was determined using an external substitution reference consisting of dioxane in D_2O at 67.66 ppm.

this study, the resonances arising from the heme propionate carbonyl carbons in cyt b_5 were used to monitor the titration of the protein with polylysine. The cyt b_5−polylysine complex is in fast exchange between its free and bound forms; consequently, the shift induced on the resonances arising from cyt b_5 upon complexation with polylysine is a weighted average of the chemical shifts corresponding to free and bound protein, as shown by eq 1.

$$\delta_o = \delta_b\alpha_b + \delta_{bp}\alpha_{bp} \quad (1)$$

The terms α_b and α_{bp} represent the fractions of free and polylysine-complexed cyt b_5, respectively. The terms δ_o, δ_b, and δ_{bp} represent the observed chemical shift at any point in the titration, the chemical shift corresponding to free cyt b_5, and the chemical shift for fully complexed cyt b_5, respectively.

The titration curve constructed by monitoring resonances arising from heme propionate carbonyl carbons (Figure 3) shows that, upon addition of polylysine to a solution containing cyt b_5, the resonances corresponding to the carbonyl carbon (▲ and ▼) located on the exposed heme edge (A6 CO and B7 CO in Figure 2) shift, whereas resonances corresponding to the carbons on the buried heme edge (A7 CO and B6 CO in Figure 2) are not affected (■

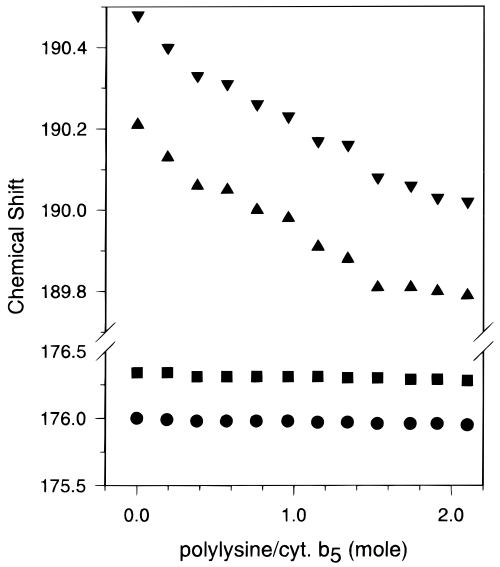

FIGURE 3: cyt b_5 with polylysine (MW = 3970). cyt b_5 resonances arising from the heme propionate located on the exposed heme edge (▲ and ▼) shift as a function of polylysine, whereas those arising from the buried heme edge (● and ■) are not affected.

and ●). These results provide strong evidence for the participation of only one of the heme propionates in cyt b_5 when it binds to polylysine and therefore confirm our postulation that the electrostatic interaction between cyt b_5 and polylysine neutralizes the negative charge on the exposed heme propionate, which results in an anodic shift in the reduction potential.

Cyclic Voltammetry. Reversible cyclic voltammograms were obtained for OM cyt b_5 or its DiMe ester at gold electrodes modified with β-mercaptopropionate in the presence of polylysine. A typical cyclic voltammogram obtained for OM cyt b_5 in the presence of polylysine (polylysine/cyt b_5 = 2.0) is shown in Figure 4. The ratio of the cathodic to anodic peak currents (i_{pc}/i_{pa}) is unity, and the peak to peak separation (ΔE_p) is 62 mV. The cathodic peak current is proportional to the square root of the scan rate, indicating that the electrochemical process is diffusion-controlled. The reduction potential values of cyt b_5 depend on the concentration and molecular weight of polylysine (Figure 5), but the attributes of the voltammograms (i_{pc}/i_{pa}, ΔE_p, and $v^{1/2}$ vs i_{pc}) remain unchanged throughout the titration with polylysine. It is also noteworthy that the potential at which the reduction potential becomes independent of the concentration of polylysine (saturation potential) also depends on the molecular weight of the polylysine (Figure 5). The positive shift in the reduction potential may be explained by the formation of a transient complex between cyt b_5 and polylysine at the electrode surface, in which the negative charge on the propionate located on the exposed heme edge is neutralized.

If neutralization of the heme propionate is the only factor modulating the reduction potential of cyt b_5, the reduction potential observed for DiMe cyt b_5, whose heme propionates are esterified, should be independent of the concentration of polylysine, as observed with the potentiometric experiments. The cyclic voltammetric experiments, however, show that the reduction potential of DiMe cyt b_5 also shifts in the positive direction as a function of the concentration of polylysine (● and ■ in Figure 5). This indicates that neutralization of the heme propionate located on the exposed heme edge is not the only factor determining the potential shift observed when the cyclic voltammetry of cyt b_5 is promoted by the addition of polylysine. An additional factor influencing the anodic shift in the reduction potential of OM cyt b_5 and its DiMe ester is discussed below.

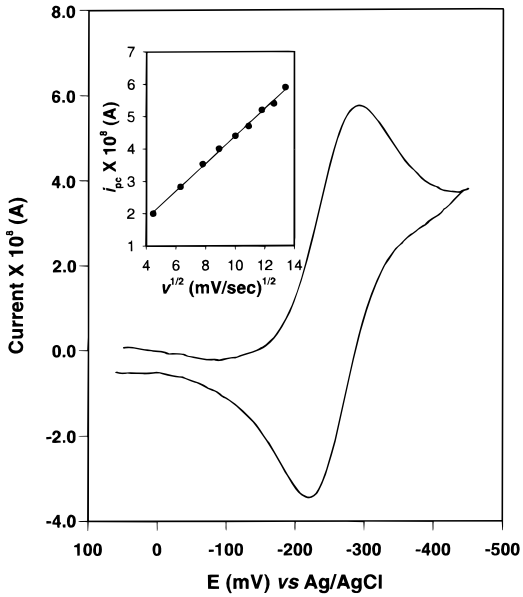

FIGURE 4: Background-subtracted cyclic voltammogram of the rat OM cyt b_5 (0.1 mM) in 100 mM MOPS at pH 7.0. The gold disk electrode was modified with β-mercaptopropionate, and the voltammogram was obtained in the presence of 0.2 mM polylysine (MW = 3970), with a scan rate of 50 mV/s. The reduction potential of OM cyt b_5 depends on the concentration and molecular weight of polylysine (see Figure 5), but the attributes for reversibility are independent of the concentration of polylysine when the polylysine/cyt b_5 ratio is larger than 0.2.

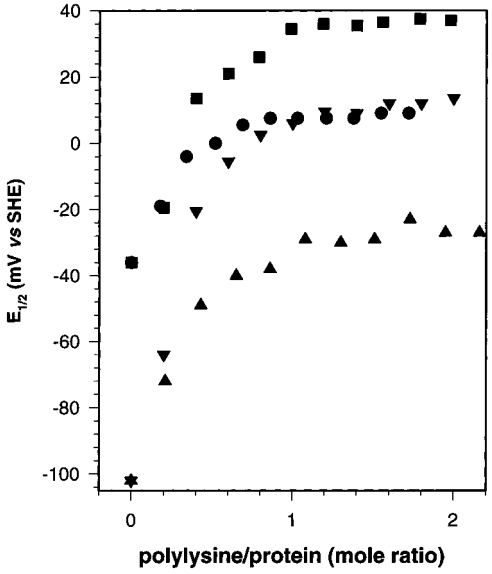

FIGURE 5: Titration of OM cyt b_5 with polylysine (MW = 3970) (▲) and with polylysine (MW = 9000) (▼). Titration of OM cyt b_5 DiMe ester with polylysine (MW = 3970) (●) and with polylysine (MW = 9000) (■). The first point in each titration curve (polylysine/protein mole ratio = 0) corresponds to the reduction potential measured by potentiometry in the absence of polylysine (see Table 1).

For electron transfer to occur at the modified electrode surface, cyt b_5 or its DiMe ester diffuses toward the electrode surface where a transient complex is formed between

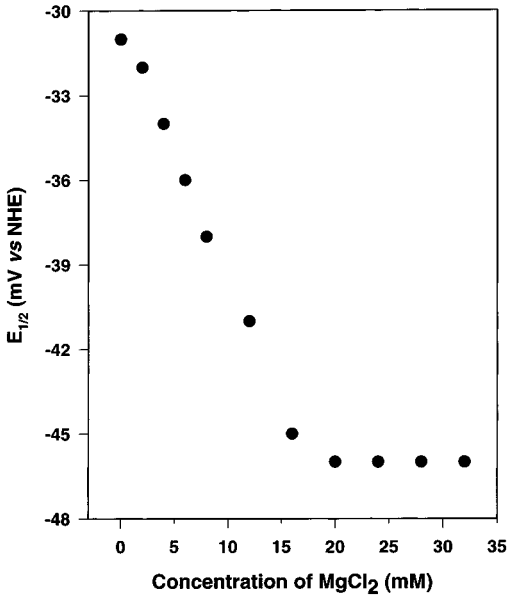

FIGURE 6: Titration of the polylysine−cyt b_5 complex (polylysine/cyt b_5 ratio = 2.0) with $MgCl_2$. The shape of the voltammograms throughout the titration was identical with the one shown in Figure 4.

polylysine and the negatively charged protein. At the scan rate used in this study (50 mV/s), diffusion of cyt b_5 toward the electrode surface is evident from the proportionality of the cathodic peak current with square root of the scan rate (Figure 4). In the transient complex formed at the electrode surface, cyt b_5 is likely to bind with polylysine utilizing its surface area delimited by acidic residues 44, 48, 56, and 60 and the heme propionate located on the exposed side of the heme (Figure 1). In fact, this is strongly supported by the ^{13}C NMR data discussed in the previous section. Consequently, water at the interface between polylysine and the protein may be excluded upon formation of the transient complex, thus decreasing the value of the dielectric experienced by the heme microenvironment. A smaller dielectric around the heme microenvironment may result in a decreased stability of the positively charged ferric heme with respect to the neutral ferrous heme, therefore contributing to the anodic shift in reduction potential. When the molecular weight of the polylysine is increased, a more positive saturation potential is observed because the larger polyelectrolyte must be capable of making a larger number of electrostatic interactions with acidic residues on the surface of cyt b_5 or its DiMe ester, thus resulting in a more efficient dehydration of the exposed heme microenvironment. Furthermore, when Mg^{2+} is added to a solution containing polylysine/cyt b_5 ratios larger than 2.0 (saturation potential in Figure 5), the reduction potential gradually shifts cathodically and saturates at approximately −47 mV (Figure 6). This indicates that Mg^{2+} competes with polylysine for the heme propionate and acidic residues on the surface of the protein. As the concentration of Mg^{2+} increases, the cyt b_5−polylysine complex dissociates and the electrochemistry is likely to be promoted mainly by Mg^{2+} ions, which have been previously shown to promote the electrochemistry of cyt b_5 at β-mercaptopropionate electrodes (*14*). The negative excursion of the reduction potential upon titration of the cyt b_5−polylysine complex with Mg^{2+} ions may be due to the increased accessibility of water to the area surrounding the exposed heme edge when the cyt b_5−polylysine complex is dissociated and the electrochemistry is promoted mainly by Mg^{2+} ions. Saturation of the reduction potential at −47 mV is likely to result from neutralization of the heme propionate negative charge upon binding to Mg^{2+}.

It has been demonstrated by Rodgers and Sligar (*33*) that the formation of a complex between cyt *c* and cyt b_5 leads to dehydration of the surface area that encompasses the exposed heme edge and that is delineated by acidic residues 44, 48, 56, and 60 and the solvent-exposed heme propionate. These investigators reported that the area at the interface of the cyt b_5−cyt *c* complex corresponds to 800 Å^2. Approximately 400 Å^2 is due to the area of buried charged side chains which provide the electrostatic interactions. The remaining 400 Å^2 of buried (dehydrated) residues is due mostly to nonpolar residues at the interface (*33*). Furthermore, McLean and Sligar (*34*) also demonstrated that, when all the charged residues proposed to form salt bridges on cyt b_5 are altered, a large negative free energy of association of the cyt b_5−cyt *c* complex still exists. These authors concluded that the main contribution to the negative free energy difference is due to a large increase in entropy which originates from the exclusion of water at the protein−protein interface (*34*). It is therefore likely that the formation of a polylysine−cyt b_5 complex, in which cyt b_5 appears to interact with polylysine utilizing its surface area delimited by the solvent-exposed heme propionate and acidic residues 44, 48, 56, and 60 (Figure 1), results in the neutralization of the exposed heme propionate and in the dehydration of the exposed heme edge, now buried at the interface, thus producing a positive shift in its reduction potential.

Crystal Structure of V45L/V61L OM cyt b_5. The initial phases for the crystal structure of the V45L/V61L mutant were solved using molecular replacement methods. The previous 2.7 Å resolution crystal structure of the wild type OM cyt b_5 (*24*) was used as the homologous search model. The molecular replacement calculation was carried out with the programs MRX (*35*) and TNT (*36*). Given the crystal lattice, there are two cyt b_5 molecules per crystallographic asymmetric unit, with a V_M of 2.6 Å^3/Da. The search for the molecular replacement solution was straightforward. The initial *R* factor with a model of two protein molecules was 0.41 for data in the resolution range of 10.0−3.0 Å.

The refinement of the crystal structure of the double mutant was carried out using the program TNT for rigid body refinement and the program X-PLOR (*37*) for simulated annealing refinement. Ten percent of the randomly selected data was used as a test data set for monitoring R_{free} (*38*). All 86 amino acid residues, one heme group of each of the two protein molecules, and 103 solvent molecules are included in the final refined model. The refinement results are summarized in Table 2. The consistency of the geometry of the crystal structure was validated using PROCHECK (*39*). All of the backbone Φ and ψ torsional angles are located withing their allowed region in the Ramachandran plot, with 93% in their most favored regions. Although noncrystallographic symmetry restraint was not applied to the model in the late stages of the refinement, the coordinates of the two protein molecules in the mutant crystal structure can be superimposed well on each other. The rms coordinate difference between C_α atoms (residues 5−80) of the two protein molecules is 0.2 Å.

Table 2: Statistics of Data Collection and Refinement for V45L/V61L

(a) data collection	
space group	$P2_12_12_1$
cell dimensions (*a*, *b*, and *c* in Å)	45.6, 71.2, and 73.8
resolution (Å)	10.0−2.0
number of unique reflections	16 374
R_{merge}[a] (%)	7.5 (27.4)[b]
completeness (%)	97.7 (84.7)
$\langle I\rangle/\sigma$	32.4 (3.4)
(b) refinement and geometry	
number of non-hydrogen atoms	
polypeptide	1386
heme group	86
solvent	103
resolution (Å)	8.0−2.0
$R_{crystal}$[c] (%)	18.0
R_{free}[d] (%)	22.4
bond length rmsd (Å)	0.007
bond angle rmsd (deg)	1.156
average temperature factor (Å^2)	
protein	37.4
heme group	39.1
solvent	50.1

[a] $R_{merge} = 100\sum|I-\langle I\rangle|/\sum I$, where I is the observed intensity and $\langle I\rangle$ is the average intensity calculated from multiple observations of the symmetry-related reflections. [b] Values in parentheses are the corresponding values in the highest-resolution shell. [c] $R_{crystal} = 100\sum||F_{obs}|-|F_{calc}||/\sum|F_{obs}|$, where F_{obs} and F_{calc} are observed and calculated structure factors, respectively. [d] R_{free} is an $R_{crystal}$ calculated using 10% test data which were chosen randomly and omitted from the subsequent refinement.

In the wild type crystal structure, the $C_{\gamma 1}$ atom of Val61 assumes a trans conformation ($\chi_1 \sim 180°$) and is 3.6 Å away from the $C_{\epsilon 1}$ atom of His63. In the mutant crystal structure, the corresponding Leu residue assumes a gauche$^+$ conformation ($\chi_1 \sim -60°$), leaving the position of the aforementioned $C_{\gamma 1}$ atom unoccupied. Similarly, the $C_{\gamma 2}$ of Val45 in the wild type structure assumes a rare gauche$^-$ conformation ($\chi_1 \sim 60°$) and is 3.9 Å away from the $C_{\epsilon 1}$ atom of His39. In the mutant structure, the position of this atom is also left unoccupied. Together, these structural changes result in a less compact packing of the heme group and the surrounding peptide chain residues at the solvent-exposed edge of the heme.

The Reduction Potential of cyt b_5 Is Lowered by Increasing the Water Accessibility to the Heme Binding Site. As mentioned previously, one edge of the heme is exposed to the aqueous environment and constitutes part of the surface of the protein together with Val45 and Val61, which are shown in light blue in panels A and C of Figure 7. It is noteworthy that, although the heme edge is exposed to the aqueous environment, the isopropyl groups of V45 and V61 (light blue in panels A and C of Figure 7) restrict the access of water to the interior of the heme cavity. When these residues are replaced by Leu, the crystal structure of the V45L/V61L mutant shows that the Leu isopropyl groups (blue in panels B and D of Figure 7) point away from the heme in order to accommodate the longer Leu side chains. The new conformation of Leu61 (blue in Figure 7D), which is located on top of the heme (red) and to the left of His63 (yellow), results in a channel that traverses the heme cavity, as shown by the white color (background) in the back of the heme. This channel is likely to provide increased water accessibility to the interior of the heme cavity. An identical view of wild type OM cyt b_5 is depicted in Figure 7C. In this view, it is apparent that the conformation of the isopropyl group of Val45 is such that access of water to the interior of the cavity is restricted. Likewise, the new conformation of Leu45 (blue in Figure 7B), which is located below the heme (red) and to the left of His39 (yellow), opens a channel to the interior of the heme cavity. In fact, Met23 (green), which is located at the deepest end of the heme cavity, is visible at the end of the channel. An identical view of the wild type protein (Figure 7A) clearly shows that the isopropyl group in Val45 restricts the accessibility of water to the interior of the heme cavity.

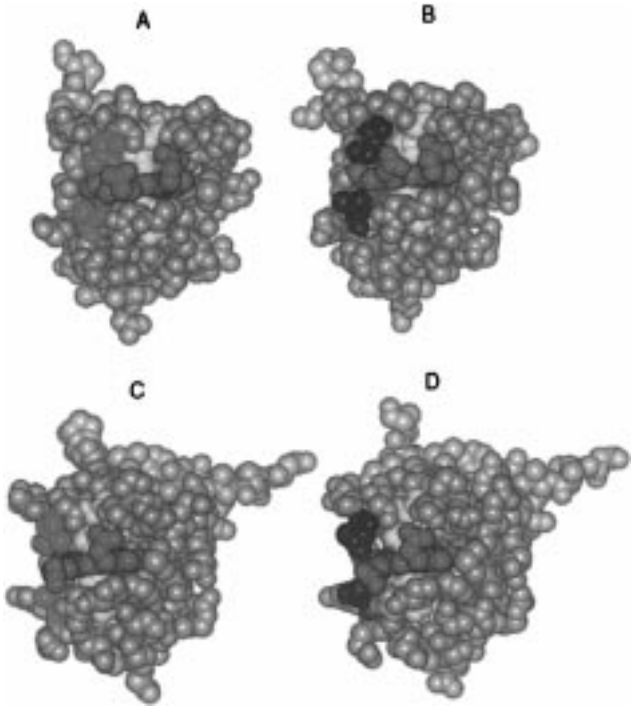

FIGURE 7: Views obtained by visualizing the coordinates from the X-ray crystal structure of the wild type and the V45L/V61L mutant of OM cyt b_5, with the aid of the program INSIGHT(II): gray, polypeptide; red, heme group; yellow, His39 and His63; green, Met23; light blue, Val45 and Val61; and blue, Leu45 and Leu61. (A) Space filling diagram of wild type OM cyt b_5. (B) Identical view of the space filling diagram of the V45L/V61L mutant of OM cyt b_5. This view shows that the isopropyl groups of L45 and L61 point away from the heme group, thus resulting in a channel leading to the interior of the heme binding site. Met23, located at the deepest end of the heme pocket, can be seen at the end of the channel. (C) Space filling diagram of the wild type OM cyt b_5. (D) Identical view for the V45l/V61L mutant in which the channel opened by the mutation traverses the heme.

The reduction potential of the V45L/V61L double mutant was measured by spectroelectrochemistry and was found to be −148 mV. By comparison, the reduction potential measured for OM cyt b_5 is −102 mV, thus corroborating the fact that an increased dielectric constant in the heme microenvironment results in a negative shift of the reduction potential of cyt b_5. The modulation of the reduction potential by the value of the dielectric constant experienced by the heme microenvironment has been documented for other heme proteins including, cyt *c* and P450. For example, it has been suggested (*40*, *41*) that the nonpolar environment of cyt *c* accounts for the fact that the reduction potential of heme in cyt *c* is 300 mV more positive than the reduction potential of heme models of cyt *c*. Subsequent theoretical models (*42*) concluded that the major source of the 300 mV

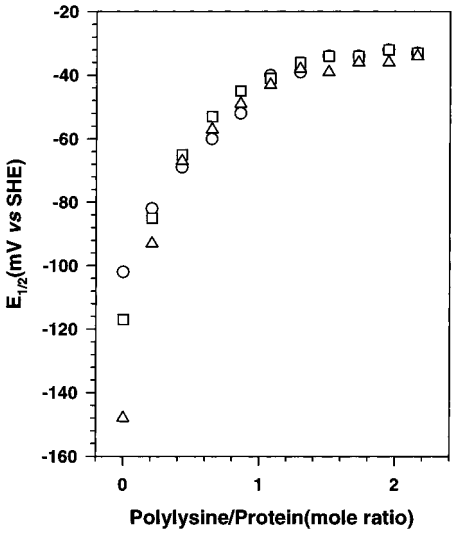

FIGURE 8: Curves for the titration of wild type OM cyt b_5 (○), the V61L mutant (□), and the V45L/V61L double mutant (△) with polylysine (MW = 3970). The first point in each of the titration curves (polylysine/protein mole ratio = 0) corresponds to the value measured by spectroelectrochemistry in the absence of polylysine.

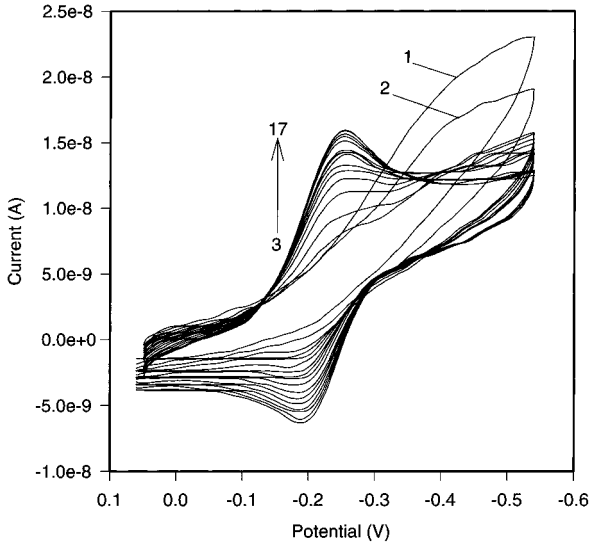

FIGURE 9: Typical cyclic voltammogram obtained for OM cyt b_5 with the aid of a glassy carbon electrode modified with a thin film of DDAB. Protein is incorporated into the cationic surfactant thin film by repetitive potential cycling until the magnitude of the current does not change. The voltammograms were obtained with a scan rate of 3 mV/s. The peak to peak separation is 59 ± 4 mV.

difference between cyt *c* and its model complexes is due to the destabilization of the positive charge on the ferric heme. The charge destabilization was attributed to the nonpolar, low-dielectric local heme microenvironment. A similar phenomenon is observed in cyt $P450_{cam}$ where the binding of camphor to the cyt P450 active site results in dehydration of the heme microenvironment, with a concomitant shift of its reduction potential from −300 to approximately −170 mV (*43*)

Implications of Measuring the Reduction Potential of cyt b_5 and Its Site-Directed Mutants Utilizing Electrodes Modified with Charged Promoters. It is often desirable to measure the reduction potential of redox proteins and that of their site-directed mutants in order to assess whether structural changes introduced by site-directed mutagenesis have an effect on their function (reduction potential). When the reduction potential of two OM cyt b_5 mutants was measured by potentiometry, the values −117 mV (V61L) and −148 mV (V45L/V61L) were obtained. However, when their reduction potentials were measured by cyclic voltammetry at a β-mercaptopropionate electrode in the presence of polylysine, the values obtained shifted in the positive direction as a function of the concentration of polylysine (Figure 8). It is striking that, although the potentiometric value of the reduction potential of the double mutant (V61L/V45L) is approximately 50 mV more negative than that measured for the wild type protein, the reduction potential values measured by cyclic voltammetry as a function of polylysine concentration are not significantly different from one another. In fact, if the measurements of reduction potential would have been carried out exclusively by direct electrochemistry methods, the relatively large difference in reduction potential between the double mutant and the wild type protein, observed with potentiometric measurements, may have been overlooked.

To further illustrate this point, the reduction potential of the wild type protein, its DiMe ester, and the V45L/V61L double mutant was measured with the aid of a glassy carbon electrode modified with a thin film of the cationic surfactant DDAB. cyt b_5 was incorporated into the cationic surfactant thin film by repeated cycling of the potential until the magnitude of the current became constant, as shown in Figure 9. The reduction potential of negatively charged proteins such as ferredoxin has been obtained with the aid of these electrodes, and the reduction potentials obtained have been in good agreement with the reduction potentials obtained by equilibrium techniques (*19*). When the reduction potentials of cyt b_5 and its derivatives are measured with the DDAB-modified electrodes, however, the reduction potentials observed are significantly more positive than those measured by potentiometry. These values are as follows: wild type OM cyt b_5, −27 mV; DiMe cyt b_5, 20 mV; and V61L/V45L, −14 mV. By comparison, the reduction potentials measured for these proteins by spectroelectrochemistry are −102, −36, and −150 mV, respectively. It is noteworthy that, when the reduction potentials of the wild type and double mutant proteins are measured with the DDAB-modified glassy carbon electrode, their difference in reduction potentials is less than 15 mV, while their reduction potentials measured by spectroelectrochemistry differ by 50 mV. Furthermore, the reduction potential of the double mutant measured with the DDAB films is more positive than that of the wild type protein, the opposite of what is observed by spectroelectrochemistry. The use of lipid films to promote the electrochemistry of redox proteins has been applied to several distinct proteins (*44*−*47*), and it appears that proteins other than cyt b_5 display reduction potentials shifted from those measured by potentiometry when lipid films are used to promote the electrochemistry in voltammetric experiments. For example, in a recent report, Zhang et al. (*48*) describe the reversible electrochemistry of cytochrome $P450_{cam}$ in biomembrane-like films, and point out that the reduction potential of cytochrome $P450_{cam}$ depends on the nature of the lipid. These authors suggest that the anodic shifts observed for cyt $P450_{cam}$ may be due to lipid-dependent double-layer effects or to protein−lipid interactions, a conclusion which may be supported by the value of the

electrode potential measured from the unpromoted electrochemistry of cyt $P450_{cam}$ at an edge-plane pyrolytic graphite electrode (*49*), which was in reasonable agreement with the potentiometric value.

Concluding Remarks. The combined evidence presented in this report, together with the unusually exposed heme in cyt b_5, indicates that the reduction potential of this protein is largely modulated by its structural properties. Modulation of the reduction potential in cyt b_5 results from the formation of a complex between cyt b_5 and polylysine, which encompasses the surface area of the protein delineated by the exposed heme propionate and acidic residues 44, 48, 56, and 60. The formation of such a complex results in (a) charge neutralization of the heme propionate on the exposed heme edge, which results in the destabilization of the positive charge on the ferric heme, thus partially contributing to the anodic shift; and (b) exclusion of water from the interface of the complex, which includes the exposed heme edge that in cyt b_5 is part of the protein surface. Exclusion of water from the complex interface may result in a significantly lower value of the dielectric experienced by the exposed heme microenvironment, thus contributing to the observed positive shift. In addition, it is also possible that double-layer effects governed by the charged promoter on the electrode surface may contribute to the modulation of the reduction potential of cyt b_5.

The sensitivity of the reduction potential to the value of the dielectric constant in the heme microenvironment of cyt b_5 was also made evident by the negative shift observed in the reduction potential of the V45L/V61L OM cyt b_5, which was found by X-ray crystallography to have an increased access of water to the heme cavity. It is also important to appreciate that the orientation of cyt b_5 in the electrostatic complexes formed with modified electrodes appears to be similar to that encountered when it binds physiological partner proteins. Since it is known that the heme propionate located on the exposed heme edge of cyt b_5 participates in electrostatic binding to cyt *c* (*24*), and that the formation of the cyt b_5−cyt *c* complex is accompanied by exclusion of water from the complex interface (*33*, *34*), it is possible that the reduction potential of cyt b_5 shifts in the positive direction when it forms a transient complex with cyt *c* before the electron-transfer event. Because the system consisting of cyt b_5 and cyt *c* has been a paradigm for the study of electron-transfer reactions among redox proteins, the possibility that the reduction potential of cyt b_5 is modulated upon formation of a transient complex with cyt *c* is worth exploring.

ACKNOWLEDGMENT

We express our gratitude to Dr. Richard Bunce for the synthesis of [1-^{13}C]ALA.

REFERENCES

1. Eddowes, M. J., and Hill, H. A. O. (1977) *J. Chem. Soc., Chem. Commun.*, 771−772.
2. Armstrong, F. A., Hill, H. A. O., and Walton, N. J. (1988) *Acc. Chem. Res. 21*, 407.
3. Taniguchi, I., Toyosawa, K., Yamaguchi, H., and Yasukouchi, K. (1982) *J. Chem. Soc., Chem. Commun.*, 1032.
4. Taniguchi, I., Toyosawa, K., Yamaguchi, H., and Yasukouchi, K. (1982) *J. Electroanal. Chem. 140*, 187.
5. Armstrong, F. A. (1990) *Struct. Bonding (Berlin) 72*, 137−221.
6. Bond, A. M. (1994) *Inorg. Chim. Acta 226*, 293−340.
7. Hawkridge, F. M., and Taniguchi, I. (1995) *Comments Inorg. Chem. 17*, 163−187.
8. Hill, H. A. O., Page, D. J., Walton, N. J., and Whitford, D. (1985) *J. Electroanal. Chem. 187*, 315−324.
9. Bond, A. M., Hill, H. A. O., Page, D. J., Psalti, I. S. M., and Walton, N. J. (1990) *Eur. J. Biochem. 191*, 737−742.
10. Bagby, S., Barker, P. D., Di Gleria, K., Hill, H. A. O., and Lowe V. J. (1988) *Biochem. Soc. Trans.*, 958−959.
11. Armstrong, F. A., Hill, H. A., and Oliver, B. N. J. (1984) *J. Chem. Soc., Chem. Commun.*, 976−977.
12. Armstrong, F. A., Hill, H. A. O., Oliver, B. N., and Walton, N. J. (1984) *J. Am. Chem. Soc. 106*, 921−923.
13. Armstrong, F. A., Hill, H. A. O., Oliver, B. N., and Whitford, D. (1985) *J. Am. Chem. Soc. 107*, 1473−1476.
14. Rivera, M., Wells, M. A., and Walker, F. A. (1994) *Biochemistry 33*, 2161−2170.
15. Glenn, J. D., and Bowden, E. F. (1996) *Chem. Lett.*, 399−400.
16. Armstrong, F. A., Cox, P. A., Hill, H. A. O., Lowe, V. J., and Oliver, B. N. (1987) *J. Electroanal. Chem. 217*, 331−366.
17. Rivera, M., Barillas-Mury, C., Christensen, K. A., Little, J. W., Wells, M. A., and Walker, F. A. (1992) *Biochemistry 31*, 12233−12240.
18. Bodman, S. B., Schuler, M. A., Jollie, D. R., and Sligar, S. G (1986). *Proc. Natl. Acad. Sci. U.S.A. 83*, 9443−9447.
19. Tominaga, M., Yanagimoto, J., Nassar, A. E. F., Rusling, J. F., and Nakashima, N. (1996) *Chem. Lett.*, 523−524.
20. Walker, F. A., Emrick, D., Rivera, J. E., Hanquet, B. J., and Buttlaire, D. H. (1988) *J. Am. Chem. Soc. 110*, 6234−6240.
21. Kurumaya, K., Okazaki, T., Seido, N., Akasaka, Y., Kawajiri, Y., and Kajiwara, M. (1988) *J. Labelled Compd. Radiopharm. 27*, 217−235.
22. Bunce, R. A., Shilling, C. L., III, and Rivera, M. (1997) *J. Labelled Compd. Radiopharm. 34*, 669−675.
23. Rivera, M., and Walker, F. A. (1995) *Anal. Biochem. 230*, 295−302.
24. Rodríguez-Marañón, M. J., Qiu, F., Stark, R. E., White, S. P., Zhang, X., Foundling, S. I., Rodríguez, V., Schilling, C. L., III, Bunce, R. A., and Rivera, M. (1996) *Biochemistry 35*, 16378−16390.
25. Teale, F. W. J. (1959) *Biochim. Biophys. Acta 35*, 543.
26. Reid, L. S., Mauk, M. R., and Mauk, A. G. (1984) *J. Am. Chem. Soc. 106*, 2182−2185.
27. Durley, R. C. E., and Mathews, F. S. (1996) *Acta Crystallogr. D52*, 65−72.
28. Guillemette, J. G., Barker, P. D., Eltis, L. D., Lo, T. P., Smith, M., Brayer, G. D., and Mauk, A. G. (1994) *Biochimie 76*, 592−604.
29. Mauk, A. G., Mauk, M. R., Moore, G. R., and Northrup, S. H. (1995) *J. Bioenerg. Biomembr. 27*, 311−330.
30. Rodgers, K. K., Pochapsky, T. C., and Sligar, S. G. (1988) *Science 240*, 1657−1659.
31. Lee, K. B., Jun, E., La Mar, G. N., Rezzano, I. N., Pandey, R. K., Smith, K. M., Walker, F. A., and Buttlaire, D. H. (1991) *J. Am. Chem. Soc. 113*, 3576−3583.
32. Rodgers, K. K., and Sligar, S. G. (1991) *J. Am. Chem. Soc. 113*, 9419−9421.
33. Rodgers, K. K., and Sligar, S. G. (1991) *J. Mol. Biol. 221*, 1453−1460.
34. McLean, M. A., and Sligar, S. G. (1995) *Biochem. Biophys. Res. Commun. 215*, 316−320.
35. Zhang, X., and Mathews, B. W. (1994) *Acta Crystallogr. D50*, 675−686.
36. Tronrud, D. E., Ten Eyck, L. F., and Mathews, B. W. (1987) *Acta Crystallogr. A43*, 489−503.
37. Brunger, A. T. (1992) in *X-PLOR version 3.1: A system for X-ray Crystallography and NMR*, Yale University Press, New Haven, CT.
38. Brunger, A. T. (1992) *Nature 335*, 472−474.
39. Laskowski, R. A., McArthur, M. W., Moss, D. S., and Thornton, J. M. (1993) *J. Appl. Crystallogr. 26*, 283−291.
40. Kassner, R. J. (1972) *Proc. Natl. Acad. Sci. U.S.A. 69*, 2263−2267.
41. Kassner, R. J. (1973) *J. Am. Chem. Soc. 95*, 2674−2677.

42. Churg, A. K., and Warshel, A. (1986) *Biochemistry 25*, 1675−1681.
43. Mueller, E. J., Loida, P. J., and Sligar, S. G. (1995) in *Cytochrome P450, Structure, Mechanism, and Biochemistry* (Ortiz de Montellano, P. R., Ed.) 2nd ed., pp 83−124, Plenum Press, New York.
44. Cullison, J. K., Hawkridge, F. M., Nakashima, N., and Yoshikawa, S. (1994) *Langmuir 10*, 877−882.
45. Nassar, A. E. F., Narikiyo, Y., Sagara, T., Nakashima, N., and Rusling, J. (1995) *J. Chem. Soc., Faraday Trans. 91*, 1775−1782.
46. Nassar, A. E. F., Willis, W. S., and Rusling, J. F. (1995) *Anal. Chem. 67*, 2386−2392.
47. Bianco, P., and Haladjian, J. (1997) *Electrochim. Acta 42*, 587−594.
48. Zhang, Z., Nassar, A. E. F., Lu, Z., Schenkman, J. B., and Rusling, J. F. (1997) *J. Chem. Soc., Faraday Trans. 93*, 1769−1774.
49. Kazlauskaite, J., Westlake, A. C. G., Wong, L. L., and Hill, H. A. O. (1996) *J. Chem. Soc., Chem. Commun.*, 2189−2190.

BI972390G